

## Modern Equations of Diffractometry. Profile Generation\*

BY D. J. THOMAS†

Medical Research Council Laboratory of Molecular Biology, Hills Road, Cambridge CB2 2QH, England, and  
European Molecular Biology Laboratory, Meyerhofstrasse 1, Postfach 10.2209, W-6900 Heidelberg, Germany

(Received 27 January 1992; accepted 22 October 1992)

### Abstract

It is possible to construct an integral which expresses the shape of diffraction spots exactly on the kinematical model, provided that phonon coupling and absorption are negligible. The integral is a function of two distributions describing quite generally the imperfections in the crystal and the beam. In the development, both the Ewald sphere and the diffraction plane are superseded by an infinitely extended quartic surface in reciprocal space reminiscent of an open tulip flower. The finite dual surface which would allow the calculation to be performed entirely in direct space is also described briefly. The method of linearizing the integral is given so that it can be used in the development and verification of profile-analysis algorithms for use with area-detector diffractometers and cameras, whether they be of the functional expansion or of the histogramming type. It is shown that in Gaussian approximation a single second-rank quantity dominates the shapes of every spot in a diffraction pattern, determining both the angular and spatial profiles simultaneously. This same approximation is the ideal zeroth-order expansion of a Weber-Hermite function profile analysis to be described in a later paper.

### 1. Introduction

This paper describes how to calculate analytically on the kinematical model of X-ray diffraction the three-dimensional shapes of diffraction spots from imperfect macroscopic crystals illuminated by imperfect beams, as measured with an area-detector diffractometer. It follows two previous ones on goniometry and on basic diffraction geometry [Thomas (1990*b*), referred to hereafter as *Goniometry*; Thomas (1992), referred to hereafter as *Geometry*]. These earlier papers reworked formal analytical and geometrical methods and addressed a range of calculations sufficient to identify and record diffraction spots on an area-detector diffractometer. The more complicated geometrical calculation of peak profiles in all dimensions

is accomplished with the help of a quartic surface in wave-vector space. This permits the development of an exact integral describing the shape of a diffraction spot on the phonon-free kinematical model subject only to the extra approximation of neglecting absorption. For reasons which will be explained later, this approximation is less contentious than it might seem. The total diffraction integral appears to be intractable in its exact quartic form, but fortunately succumbs readily enough to linearization without material loss of accuracy. When the properties of the total diffraction integral are examined under Gaussian approximation to the controlling distributions, it is seen that the basic shape of every spot is controlled by a single second-rank quantity called III (shah). This result has been demonstrated before for the angular diffraction widths of a point-like crystal [when III appears in an incomplete tensor-like form (Thomas, 1982; *Geometry*)] and the result survives even when the crystal is not vanishingly small. As shown here, the full form of the same quantity describes the cross section of the scattered beam within the same approximation. The symbols for this section are given in Table 1.

The Gaussian results are the ideal zeroth-order expansion of a Hermite-function-based profile analysis which will be described in greater detail in a later paper. Profile analysis is destined to become increasingly important as ever greater demands are placed on inevitably imperfect area detectors with their relatively broad point-spread functions (see Thomas, 1990*a*) and as ever larger biological macromolecules are crystallized. The reason why profile analysis is supposed to be advantageous is that it downweights the tails of diffraction spots where the data are relatively more noisy. However, great care has to be exercised to ensure that the expectation spot shape is accurate, lest significant but undetectable systematic bias be introduced. Diamond (1969) also points out that one of the practical advantages is more basic: that determinations of peak intensities from profile analysis and from 'shoe-box' (the area-detector equivalent of 'background-peak-background') measurements can be compared, and a large difference is a good indication of an unreliable measurement. It is hoped that the geometrical analysis given here will be useful in establishing the extent to which current algorithms depending on assumptions of local similarity [e.g. the implementation of Kabsch (1988)] are trustworthy and in providing the basis for more global approaches

\* This paper is a sequel to Modern Equations of Diffractometry. Goniometry [*Acta Cryst.* (1990), A46, 321–343] and Modern Equations of Diffractometry. Diffraction Geometry [*Acta Cryst.* (1992), A48, 134–158].

† Present address: European Molecular Biology Laboratory.

Table 1. *Symbol table for § 1*

$\cdot$	missing argument of a function
$\cdot\int\cdot$	the rotationally skew-symmetric operator defined in <i>Goniometry</i>
$\cdot\perp\cdot$	rank 2 projective operator developed from the rotationally symmetric operator ( <i>Goniometry</i> )
$\cdot\lrcorner\cdot$	rank 1 projective operator developed from the rotationally invariant operator ( <i>Goniometry</i> )
$\cdot\hat{\cdot}$	a quantity like a pointer or a signed axis, whose magnitude has no relevance ( <i>Goniometry</i> )
$\hat{\cdot}, \hat{\cdot}$	a rotation operator, and its inverse ( <i>Goniometry</i> )
$ \cdot $	the absolute value
$\ \cdot\ $	the Euclidean norm of a vector or covector
$[\cdot], [\cdot]$	operator having the same effect as a vector cross product, and its inverse ( <i>Geometry</i> )
$\langle\cdot, \cdot\rangle$	vector in reciprocal space as left and right multiplicands
$(\cdot, \cdot)$	vector in small-angle vector space as left and right multiplicands; generically $\hat{\cdot}$
$\{\cdot, \cdot\}$	vector in direct space as left and right multiplicands
$\overline{\cdot}$	(overline) a generalized matrix inverse (Moore, 1920, 1935; Penrose, 1955)
$\iiint d^3\cdot$	a volume integral

based on either Weber-Hermite functional expansions or direct three-dimensional histogramming, as is sometimes preferred.

The contracted notation here follows the two previous papers closely and assumes an even greater importance, as will be seen, for example, in §8 which would be intolerably expansive in full component notation. Three spaces are used explicitly throughout. These are reciprocal space, direct space and small-angle vector space. In each case, a Dirac-like (*cf.* Dirac, 1958) notation is used to denote vectors but the three types of vector are distinguished by differing brackets. Thus  $\cdot\cdot$  is used in reciprocal space,  $\cdot\cdot$  in direct space and  $\cdot\cdot$  in small-angle vector space. These are complemented by variously symmetric rotational operators such as  $\cdot\int\cdot$ ,  $\cdot\perp\cdot$  and  $\cdot\lrcorner\cdot$  as expounded in *Goniometry*. A brief résumé of the geometry of these operators is given in Fig. 1.

A fourth space (of directions, characterized by  $\cdot\hat{\cdot}$ ) is also used here, but for the most part appears only implic-

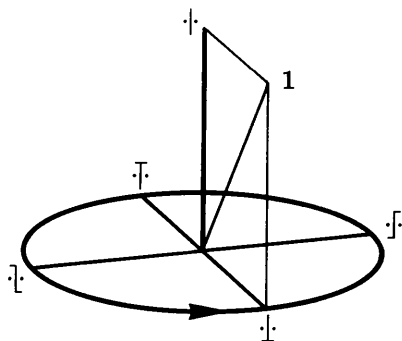


Fig. 1. An indicator diagram for the rotational operators. This shows geometrically the invariant operator  $\cdot\int\cdot$  which projects its vector argument onto a line such as an axis of rotation, and the skew operators  $\cdot\lrcorner\cdot$  and  $\cdot\perp\cdot$  which project their vector arguments onto a plane such as an orbital plane as shown here with an attendant right rotation. The symmetric operator  $\cdot\perp\cdot$  similarly projects onto the same plane, but with no attendant rotation, whilst the antisymmetric operator  $\cdot\lrcorner\cdot$  projects with a rotation of half a turn. The identity operator, 1, marks the unaltered operand in its original position.

itly. The vector cross product appears within the same consistent framework as a second-rank operator,  $[\cdot] = \cdot\int\cdot \|\cdot\|$ . The consequent unusual appearance of some of the equations is, of course, superficial and is offset by their greater power, compactness and (with practice) ease of use. The operators  $\cdot\int\cdot$  and  $\cdot\perp\cdot$  are used in a more general way here than in *Goniometry* by allowing the two occurrences of the argument to differ.

This paper makes extensive use of covectors as well as vectors. It is hoped that Figs. 2 and 3 will provide a sufficient summary of the relevant geometrical properties. All three figures for this *Introduction* are reproduced from the earlier papers, where a fuller explanation can be found.

## 2. Basic definitions

This paper is concerned mainly with a demonstration of the major effects generating the profiles in all dimensions of diffraction spots measured on an area-detector diffractometer such as the Enraf-Nonius FAST system (a television diffractometer with a solid-state detector), with an electronic camera using phospholuminescent imaging plates (PIPs) or multiwire proportional counters (MW-

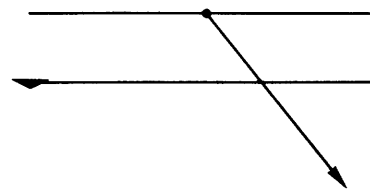


Fig. 2. The action of a covector upon a vector. Covectors are represented faithfully and naturally by a series of contour planes. Here, a covector acting on a vector is represented by a downhill contour intersecting the tail of the vector and by an uphill contour one unit higher marked with a broad arrowhead. The value of the product is the number of contour levels between the head and the tail of the vector, which is  $2\frac{1}{2}$  in the case illustrated. It is characteristic of this representation that larger covectors have their contours closer together. Perhaps it takes some time to accommodate this apparent perversity, but it is quite sensible when it is realised that it is the density of contour lines that is proportional to the magnitude of the covector.

PCs). As such, the contribution from all inelastic scattering events including those which couple to phonons are ignored, following normal X-ray convention in all but the most fastidiously executed work. Phonon coupling is much more important in neutron diffraction and the approximations made here would generally not be regarded as acceptable for that application. Absorption is also neglected here because it demands a much more complicated analytical treatment but is generally less important when working with neutrons which interact with matter even more weakly than do X-rays. However, the modern trend towards the use of Mo  $K\bar{\alpha}$  or shorter-wavelength synchrotron radiation instead of Cu  $K\bar{\alpha}$ , the increasing tendency to struggle with very small crystals and the occasional use of a filled capillary (Richmond, Finch, Rushton, Rhodes & Klug, 1984) all reduce the impact of differential absorption on the spot profiles. It is assumed here that the characteristically broad tails under spots caused by phonon coupling (*i.e.* thermal diffuse scattering, or TDS) and the effects of absorption can both be accommodated adequately by the full profile analysis to follow in a later paper. The symbols for this section are given in Table 2.

Kinematical diffraction geometry in the absence of phonon coupling is dominated by equations of conservation of momentum,  $\langle S \rangle = \langle R \rangle - \langle T \rangle$  [*Goniometry*, (11.1); *Geometry*, (3.1)], and of energy,  $\langle SS \rangle = \langle TT \rangle$  [*Goniometry*, (11.2); *Geometry*, (3.2)]. First eliminating the scattered beam,  $\langle T \rangle$ , and then making a couple of minor rearrangements reduces these to the equalities

$$\langle RR \rangle = 2\langle RS \rangle = 2\langle RT \rangle = 4\langle SR|RT \rangle, \quad (2.1)$$

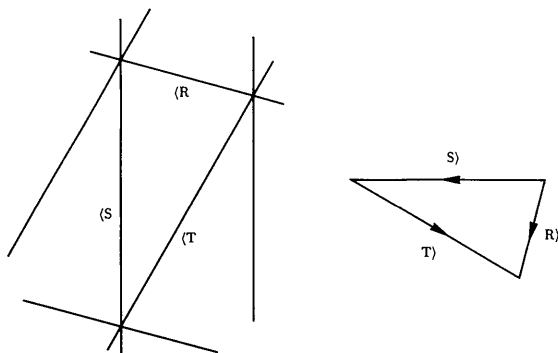


Fig. 3. Basic diffraction geometry as covectors or as vectors. The covector diagram on the left displays most clearly the balance of periodicities between  $\langle S \rangle$ ,  $\langle T \rangle$  and  $\langle R \rangle$  in direct space. The 'direction' or 'sign' of each covector is marked by the positioning of its label, which occupies the more positive side of an arbitrary contour (this is somewhat simpler than the method used by Burke, 1985). The equivalent conjugate diagram (on the right) using vectors in reciprocal space is much more familiar. The vector,  $\langle S \rangle$ , is defined to point in the direction from the crystal to the source, and thus in the opposite direction to the motion of the photons. This choice is justified on several grounds: it is convenient to use the nominal crystal position as the origin for all quantities in direct space; the equations, fortuitously, have fewer minus signs; perhaps more importantly, there is a direct analogy with the analytical quantum-mechanical formula for the scattering event, where the incoming photon being destroyed and the newly created outgoing photon appear in mutually conjugated forms.

which are used frequently to simplify other results. As is very well known, when  $\langle S \rangle$  is held fixed, the solution for  $\langle R \rangle$  of the first equation [referred to simply as 'the diffraction condition': *cf. Goniometry*, (11.3); *Geometry*, (3.3)] is a sphere centred on  $\langle S \rangle$  named after Ewald (1913). Fixing  $\langle R \rangle$  gives the equally well known diffraction plane on which  $\langle S \rangle$  bisects  $\langle R \rangle$ ; though this is more commonly used in the study of neutron diffraction.

Neither of these familiar surfaces is particularly helpful for profile analysis on an area detector, however, when it is much more pertinent not to fix  $\langle R \rangle$ ,  $\langle S \rangle$  or even  $\langle T \rangle$ , but rather the detected position of the 'scattered' photon.† This can be denoted by the two-dimensional vector  $\langle Q \rangle$  or its three-dimensional extension  $\langle Q^* \rangle$  (Thomas, 1989), both of which (by definition) lie within the assumed detection plane (Thomas, 1989); thus, even the three-dimensional  $\langle Q^* \rangle$  can span only a two-dimensional subspace. To allow the discussion of small changes not necessarily constrained to lie in this subspace, an equivalent vector,  $\langle \Theta \rangle$ , is used here.  $\langle Q^* \rangle$  and  $\langle \Theta \rangle$  are both tied to the crystal and are always parallel. The name  $\langle \Theta \rangle$  is chosen to draw attention to the relationship that this vector along the scattered beam bears to the Bragg angle (Bragg, 1913),  $\theta$ , which finds no direct application in the theory of area diffractometry (*Geometry*). This is fortunate because some representation of the position on the detector must be an argument in the equations for beam cross section; the conveniently compact symbol  $\langle \vartheta \rangle$  can then be used without any risk of confusion to denote a small (but not generally infinitesimal) shift in any direction away from the central position of the diffracted beam,  $\langle \Theta \rangle$ , which would otherwise be written  $\delta\langle \Theta \rangle$ .

It will turn out that terms of the type  $\langle T \rangle \langle R \rangle / \langle RT \rangle$  occur quite frequently and it is helpful to contract them in a natural extension of the notation for the rotationally invariant operator  $\langle \cdot | \cdot \rangle$ , using the definition

$$T|R = \frac{\langle T \rangle \langle R \rangle}{\langle RT \rangle}. \quad (2.2)$$

This is clearly consistent with the definition of the previously symmetric  $\langle \cdot | \cdot \rangle$  when the two arguments ( $\langle T \rangle$  and  $\langle R \rangle$ ) are the same. The same property of being independent of the magnitude of the arguments is preserved and the new operator is also considered to be a rank-one quantity. It nulls any vector on the right which is contained within the zero contour of  $\langle R \rangle$ , which is equivalent in Cartesian-

† Kabsch (1988) has nonetheless developed a practical method of profile analysis based on the idea of mapping the perceived shapes of the spots back onto local regions of the Ewald sphere. In this regard, Kabsch follows Diamond (1969) who also preferred a numerical histogramming approach for the linear diffractometer (Arndt & Phillips, 1961) based on a (clearly justifiable) assumption of locally similar geometry. Both of these implementations are renowned for their reliability. This paper addresses the different question of trying to relate the perceived shapes directly to the fundamental controlling distributions describing the beam and the crystal. The contribution from the detector is deferred to the next paper, but can to some extent be anticipated from the discussion in Thomas (1990a).

Table 2. *Symbol table for § 2*

<b>1</b>	the multiplicative identity, representable as a unit matrix
$\alpha$	factor relating direct-space and reciprocal-space representations of a scattered beam
$b\}$	a short vector in direct space, referred to the crystal
$\theta$	the Bragg angle
$\bar{\mathbf{F}}$	the oriented conventional reciprocal-space unit cell
$h$	Miller indices, $(h, k, \ell)$
$H\}$	any vector pointing in the same direction as $\Theta\}$ or $T\}$
$\mu$	a mosaic misorientation angle
$\check{\mu}$	small-angle vector representing rotation through a mosaic misorientation angle
$\bar{\mathbf{M}}$	a mosaic misorientation axis
$\bar{\mathbf{M}}, \hat{\mathbf{M}}$	operator effecting rotation through a mosaic misorientation angle, and its inverse
$p\}$	a short vector in direct space, referred to the laboratory
$\psi$	the (Arndt-Wonacott) diffraction angle (Arndt & Wonacott, 1977)
$\bar{\Psi}$	a signed representation of the axis of total rotation from datum
$\hat{\Psi}, \check{\Psi}$	rotation through $\psi$ , and its inverse
$\phi$	a very small perturbation in the diffraction angle (about $\bar{\Phi}$ )
$\check{\phi}$	a small-angle vector denoting a small rotational perturbation away from the diffracting position
$\bar{\Phi}$	a signed representation of the instantaneous axis of rotation ( <i>i.e.</i> axis of angular velocity)
$\hat{\Phi}$	rotation through $\phi$ about $\bar{\Phi}$
$Q$	a point on the detector faceplate as a 2-vector; also $Q^*$ as a 3-vector
$\Theta\}$	the scattered beam in direct space; $\Theta\} \parallel Q^*$
$\vartheta\}$	a small variation in $\Theta\}$
$R\}$	a Bragg plane in the diffracting position
$S\}$	a reversed incident-beam wave vector
$T\}$	the scattered-beam wave vector
$X\}$	a Bragg plane, referred to the crystal frame

Euclidean space to saying any vector perpendicular to  $R\}$ . Similarly, it nulls any covector multiplying on the left whose zero contour contains  $T\}$ . A similar argument about perpendicularity holds in Cartesian-Euclidean space.

The Miller indices,  $h$ , and hence the magnitude (*i.e.* length) of the reciprocal-lattice vector,  $R\}$ , must be known from the outset since  $R\}$  is given by

$$R\} = \hat{\Phi}\hat{\Psi}\bar{\mathbf{M}}X\}, \quad (2.3)$$

extending equation (11.4) in *Goniometry* to allow for the possibility of crystal mosaicity. The operator  $\hat{\Psi}$  describes the total rotation of the crystal through an angle  $\psi$  about the axis  $\bar{\Psi}$  from its datum position to the nominal central diffraction position of the spot being considered:

$$\hat{\Psi} = \Psi|\bar{\Psi} + \Psi\check{\Psi} \sin \psi + \Psi\check{\Psi} \cos \psi. \quad (2.4)$$

Derivations of  $\psi$  in this notation can be found in *Goniometry* and in *Geometry*, though both are derivative expositions based on Wonacott (1977). The rotation operator  $\hat{\mathbf{M}}$  effects the mosaic-block rotation specified by the small-angle vector  $\check{\mu}$  following the same method as is given in §9 of *Goniometry*:

$$\mathbf{M} = \mathbf{M}|\check{\mu} + \mathbf{M}\check{\mathbf{M}} \sin \mu + \mathbf{M}\check{\mathbf{M}} \cos \mu; \quad \mu = \|\check{\mu}\|; \quad \bar{\mathbf{M}} = \frac{\check{\mu}}{\mu}. \quad (2.5)$$

The expectation value of  $\hat{\mathbf{M}}$  is **1**, based on an assumption

that the unit-cell matrix,  $\bar{\mathbf{F}}$ , defined below will be refined correctly at all times. All of the Jacobian derivatives necessary to do this have already been given in the two previous papers.  $\hat{\Phi}$  is also a rotation operator specified from a small-angle vector and (following the usage in *Geometry*) describes a deliberate missetting of the crystal away from the central diffraction position, again expressed conveniently as a function of a small-angle vector  $\check{\phi}$ :

$$\hat{\Phi} = \Phi|\check{\phi} + \Phi\check{\Phi} \sin \phi + \Phi\check{\Phi} \cos \phi; \quad \phi = \|\check{\phi}\|; \quad \bar{\Phi} = \frac{\check{\phi}}{\phi}. \quad (2.6)$$

At the central diffraction position  $\hat{\Phi} = \mathbf{1} = \bar{\Phi}$ , which much simplifies many of the equations given later. The reciprocal-space vector  $X\}$  also follows the definition given earlier [*Geometry*, (3.11)] in the transposed form:

$$\langle X = \langle h\bar{\mathbf{F}} = (h, k, \ell) \begin{bmatrix} \langle h\bar{\mathbf{F}} \\ \langle k\bar{\mathbf{F}} \\ \langle \ell\bar{\mathbf{F}} \end{bmatrix}, \quad (2.7)$$

which was written this way only because  $\bar{\mathbf{F}}$  is defined as the inverse of the matrix representing the conventional direct-space unit cell,  $\mathbf{F}$ , so that  $\bar{\mathbf{F}}$  has its component triplet of vectors in the rows rather than in the columns, as in  $\mathbf{F}$ . The equivalent well known **UB** matrix of Busing & Levy (1967) is transposed relative to the usage here. Apart from

specifying what is meant by  $X$ ), the Miller indices,  $h$ , are not otherwise needed in this paper.

Vectors in direct space tied to the crystal are also needed in a form referred to the laboratory frame. A small displacement from the nominal crystal centroid is used frequently and the two forms are related by

$$p\} = \hat{\Phi}\hat{\Psi}b\}; \quad (2.8)$$

$b\}$  is tied to the crystal and  $p\}$  to the laboratory. The  $\hat{\Phi}$  operator actually has very little effect here since  $\phi$  and  $b\}$  are both small (say of order  $\delta$ ) by definition.

### 3. The diffraction tulip

To calculate the total diffracted intensity at a given point on the detector, it will be necessary to integrate over all positions within the crystal and over all mosaic angles, leaving  $S\}$  as the only unknown quantity.\* The solution sought for  $S\}$  represents the incident photons that could strike the given position on the detector by being diffracted from the periodicity (reciprocal-lattice vector)  $X$ ). To find  $S\}$ , it is necessary to demand that the reciprocal-space representation of the scattered beam,  $T\}$ , be parallel to the direct-space representation of the scattered beam emanating from a position  $p\}$  within the crystal and landing at  $\Theta\} + \vartheta\}$  on the detector:

$$T\} = \frac{1}{\alpha} (\Theta\} + \vartheta\} - p\}) \equiv |\Theta + \vartheta - p\}| / \alpha. \quad (3.1)$$

Here,  $\alpha$  has the dimensions of area (usually with mixed units) and is the same symbol as in the previous simplified equation (5.1) of *Geometry*. Typically, the unit cell is measured in ångstrom units, Å, and the diffractometer in mm, so the mixed units of  $\alpha$  are then Å mm. The thin vertical line here delimits the sum of vectors in direct space rather than indicating a direction. Substituting the equation into the equation of momentum balance gives

$$S\} = R\} - |\Theta + \vartheta - p\}| / \alpha, \quad (3.2)$$

which can be premultiplied by  $\langle R$  and simplified using the equation of the diffraction condition (2.1) to give

$$\frac{1}{\alpha} = \frac{\langle RR \rangle}{2 \langle R | \Theta + \vartheta - p \rangle}. \quad (3.3)$$

\* The baldness of this sentence, which affects the entire development of this paper, is somewhat disingenuous. The author was led to the conclusion expressed by writing the shape of a diffraction spot as a total integral over all quantities,  $R$ ),  $S$ ),  $T$ ),  $\mu$  and  $b\}$  or  $p\}$ . The integral was set up with Dirac  $\delta$  functions to constrain the integrand to obey all of the relevant equalities, and the author was then unable to find any workable reduction except for the one used here. In a way this is rather satisfactory, because the workable set of variables also seems to be the most natural one.

Substituting this value back into (3.2) gives the required result:

$$\begin{aligned} S\} &= R\} - \frac{|\Theta + \vartheta - p\} \langle RR \rangle}{2 \langle R | \Theta + \vartheta - p \rangle} \\ &= \hat{\Phi}\hat{\Psi}\hat{M}X\} - \frac{|\Theta + \vartheta - \hat{\Phi}\hat{\Psi}b\} \langle XX \rangle}{2 \langle X\hat{M}\hat{\Psi}\hat{\Phi} | \Theta + \vartheta - \hat{\Phi}\hat{\Psi}b \rangle}, \end{aligned} \quad (3.4)$$

in which the substitutions (2.3) and (2.8) have been used. The six rotation matrices that would be between  $\langle X$  and  $X \rangle$  cancel to the identity. The magnitude of the solution for  $S\}$  is clearly directly proportional to  $\|R\| \equiv \|X\|$ , but depends only on the direction of  $|\Theta + \vartheta - p\}$ . For this reason,  $|\Theta + \vartheta - p\}$  could be replaced with impunity in (3.4) by  $T\}$ , or indeed any other vector  $H$ ) of non-vanishing magnitude pointing in the same direction. Making this latter substitution, multiplying out the denominator and then rearranging shows that

$$\langle S \rangle^2 \langle H - R \rangle^2 \langle H + H \rangle \langle R \rangle = 0. \quad (3.5)$$

This can be squared, resulting in an equation quadratic in  $S\}$  and quartic in  $R\}$  whose solution for  $S\}$  is a doubly branched infinitely long test-tube-shaped surface axially symmetric about  $H$ ). The region near the origin has the greater practical importance (corresponding to moderate and large Bragg angles) and has a shape reminiscent of an open tulip flower, after which the surface is named. See Fig. 4.

The curvature of the tulip is highest at its tip, whose sphericity and radius of  $\|R\|/2$  are both characteristic of back scattering. Its infinitely extended cylindrical end has a radius of curvature asymptotically equal to  $\|R\|$ , which features are characteristic of small-angle scattering.

If the reciprocal-lattice vector and the scattered-beam vector rotate in step, the tulip, the diffraction plane and the Ewald sphere just co-rotate. If the two vectors rotate relative to each other, the Ewald sphere changes size as well because the solution for  $S\}$  changes magnitude.

The shape of the tulip is calculated most easily in the form of a parameterized curve representing a central two-dimensional section as shown in Fig. 5 in which  $\langle H = [0, 1, 0]$ ,  $\langle R = [r \sin \vartheta, r \cos \vartheta, 0]$  and  $\vartheta$  is the complement of the Bragg angle,  $\theta$ . Then the parametric form

$$\begin{aligned} \langle S &= [x, y, 0] \\ &= [r \sin \vartheta, r \sqrt{\left(\frac{\sec^2 \vartheta}{4} - \sin^2 \vartheta\right)}, 0] \end{aligned} \quad (3.6)$$

follows directly from the figure. The outer rectangle in Fig. 5 has width  $\sqrt{r^2 - x^2} = r \cos \vartheta$  and height  $\sqrt{x^2 + y^2} \sin 2\vartheta = r \sin \vartheta$ , so its area can be expressed as

$$\begin{aligned} \sqrt{x^2 + y^2} \sin 2\vartheta \sqrt{r^2 - x^2} &= r \sin \vartheta r \cos \vartheta \\ &= \frac{r^2}{2} \sin 2\vartheta. \end{aligned} \quad (3.7)$$

Cancelling  $\sin 2\vartheta$  and squaring gives the non-parametric equation to which (3.6) is a solution:

$$(x^2 + y^2)(r^2 - x^2) = \frac{r^4}{4}. \quad (3.8)$$

The unneeded second branch induced by squaring corresponds to Bragg angles whose magnitude exceeds  $90^\circ$ ; this just means that  $H$ ) points in the wrong direction.

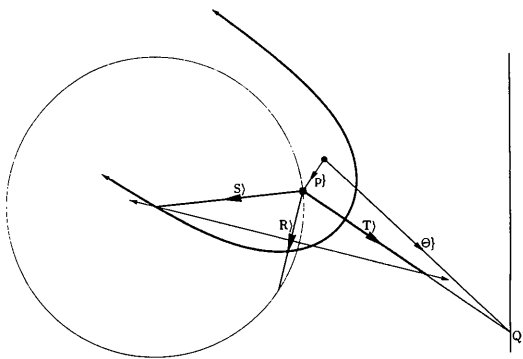


Fig. 4. The diffraction tulip. This figure displays diffraction geometry in direct space and in reciprocal space simultaneously. The origin of direct space, being the nominal crystal position and rotational centre of the goniostat, is marked with a small circle. The origin of reciprocal space, coinciding with the direct-space volume element at  $p$ ), is marked with a square. The bold curve is a section of the diffraction tulip introduced in this paper, a surface axially symmetric about  $T$ ) defining the locus of all incident-beam reversed wave vectors which could be diffracted by  $X$ ) at some orientation of the crystal and then land at  $Q^*$ ). The fine line to the right denotes the assumed plane of detection of the X-rays.  $S$ ) is the specific solution when  $X$ ) is rotated into the position  $R$ ) and an appropriate elementary Ewald sphere is shown very lightly. The diffraction plane which bisects  $R$ ) is also shown lightly. If the diagram were treated as a calculating device, it would operate as follows: define the position of interest,  $Q^*$ , on the detector and the position  $p$ ) of a small part of the crystal; the line between these defines  $H$ ) which is also the axis of the tulip; decide which diffraction spot is to be studied and evaluate  $||X||$  for it, which sets the size of the tulip; then any point on the surface of the tulip represents an incident reversed wave vector which could be diffracted onto  $Q^*$  by  $X$ ); it will do so when the crystal is so oriented that  $X$ ) is  $R$ ) =  $S$ ) +  $T$ ).

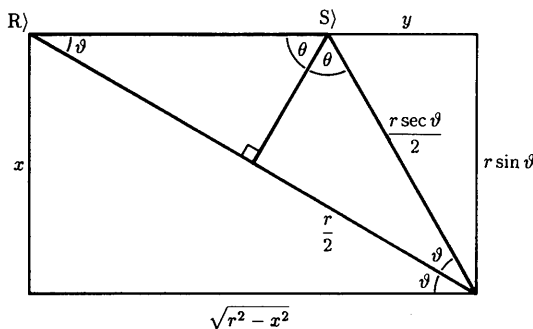


Fig. 5. A central section of the tulip. This shows the parameterized geometry of a central section of the diffraction tulip.  $\vartheta$  is the complement of the Bragg angle  $\theta$ . The scattered beam  $T$ ) is horizontal, along the  $y$  axis, and  $x$  is used as a typical radius vector. The origin to which  $R$ ) and  $S$ ) are tied is at the lower right corner.

#### 4. The equivalent direct-space representation of diffraction

Although it is usual to discuss diffraction geometry with the help of constructions in reciprocal space, it must be possible to achieve the same results entirely in direct space. The most natural way is by the use of a cam-like device whose surface has the property of determining the position of a wave crest one wavelength away from the origin of the figure, as shown in bold lines in Fig. 6. The calculations of this section are not used later, and for simplicity are given in a two-dimensional parametric form, so rows represent covectors and columns represent vectors. Everything scales together if all of the working is in the same space, so the procedure is to define the plane of the diffractable incident wave by the unit covector  $[\cos 2\theta, \sin 2\theta]$  where  $\theta$  is the parametric Bragg angle. With the assumption that any point on the surface of the cam may be called  $[x, y]^T$ , the distance between this point and the wavefront intersecting the origin must be the wavelength sought,  $\lambda$ , which is also determined by Bragg's law:

$$[\cos 2\theta, \sin 2\theta] \begin{bmatrix} x \\ y \end{bmatrix} = \lambda = 2d \sin \theta$$

$$\Rightarrow f(x, y, \theta) = x \cos 2\theta + y \sin 2\theta - 2d \sin \theta = 0. \quad (4.1)$$

The rearrangement of the equation into the form of an implicit (*i.e.* constant) function means that a required extra

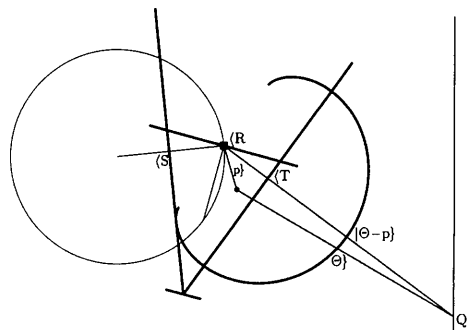


Fig. 6. The diffraction cam. This diagram is in direct space except for the lightly drawn Ewald sphere, scattering vector  $R$ ) and solution for the reversed source wave vector,  $S$ ), which are not needed in the construction. The covectors representing the periodicities of the Bragg planes and of the incident and re-radiated beams are magnified enormously relative to the vectorial depiction of the same beams and of the assumed plane of detection. The reciprocal-space construction is scaled so that the apparent length of  $R$ ) equals the separation of the Bragg planes. Its operation as a calculating device follows that for the tulip very closely. The position of the detected photon,  $Q^*$ , a position within the crystal,  $p$ ), and the magnitude of a reciprocal-lattice vector,  $||X|| = ||R||$ , define the cam and then any plane tangential to it is the position of the last wave crest of a scatterable incoming wave before the one which contains the origin (*i.e.* the +1 contour of the covector  $S$ ) which points into the source). The scattered beam is represented by the first wave crest after the one containing the origin (*i.e.* the +1 contour of the covector  $T$ ). The unnecessary zeroth contours of  $S$ ) and of  $T$ ) are not shown. The Bragg planes are represented by contours 0 and +2. The missing contours tend to confuse the diagram.

Table 3. *Symbol table for § 5*

$\frac{1}{2}$	the halving operator, representable as half a unit matrix; extendable to any other fraction
$c$	the speed of light
$e$	the electronic charge
$F$	a structure factor
$I$	the predicted intensity profile of a diffraction spot
$ L $	the conventional Lorentz factor
$m$	the mass of an electron
$p$	the conventional polarization factor
$Q^{2(3)}$	the vector space spanned by $Q$ , which includes the detection plane
$s)$	a small variation in $S)$
$\langle U$	the normal to the surface of the diffraction tulip
$\delta V$	a small volume element
$\lambda$	the wavelength of the radiation, usually X-rays
$\Sigma$	the beam wave-vector distribution
$\Xi$	the mosaicity distribution within the crystal, as a function of mosaic misorientation angle
$\Upsilon$	the antisymmetric form $\langle S\Phi \Phi R\rangle = \langle R\Phi \Phi S\rangle = -\langle R\Phi \Phi S\rangle = -\langle S\Phi \Phi R\rangle = L^{-1}$
III	(shah) a second-rank (bi-covector-like) tensor form describing angular diffraction widths

equation can be created by setting the differential  $df = 0$  as well:

$$0 = df = [-2x \sin 2\theta + 2y \cos 2\theta - 2d \cos \theta] d\theta + \cos 2\theta dx + \sin 2\theta dy. \quad (4.2)$$

The lower line can, and indeed should, be set to zero independently:

$$\cos 2\theta dx + \sin 2\theta dy = 0, \quad (4.3)$$

since it demands that the sought wavefront be tangential to the cam (see Fig. 6). Thus, (4.2) reduces to

$$-x \sin 2\theta + y \cos 2\theta = d \cos \theta, \quad (4.4)$$

which combines with (4.1) to give

$$\begin{bmatrix} \cos 2\theta & \sin 2\theta \\ -\sin 2\theta & \cos 2\theta \end{bmatrix} \begin{bmatrix} x \\ y \end{bmatrix} = \begin{bmatrix} 2d \sin \theta \\ d \cos \theta \end{bmatrix} \quad (4.5)$$

whose solution is

$$\begin{bmatrix} x \\ y \end{bmatrix} = \begin{bmatrix} \cos 2\theta & -\sin 2\theta \\ \sin 2\theta & \cos 2\theta \end{bmatrix} \begin{bmatrix} 2d \sin \theta \\ d \cos \theta \end{bmatrix}. \quad (4.6)$$

This curve has a characteristic shape rather like the aerial surface of a droplet sitting on a surface. Unlike the tulip, whose open end extends to infinity to meet the second branch, the drop-shaped surface is closed on a perfectly formed rim within a plane containing the origin of Fig. 4. These contrasting properties are not accidental: the tulip is constructed entirely with vector geometry in reciprocal space, whilst the cam is the same construction made entirely with the dual covector geometry in direct space; therefore, the two surfaces must be duals.

### 5. The contribution to the scattered intensity from a small part of the crystal

The symbols for this section are given in Table 3. It is necessary to be able to describe first the scattering from a very tiny part of a crystal before tackling the more complex calculations relating to the whole crystal. Lipson (1972) says that the intensity diffracted from a small part of a crystal is equal to

$$\frac{1}{|L|} \left( \frac{Ne^2|F|}{mc^2} \right)^2 \lambda^3 \frac{1 + \cos^2 2\theta}{p} \delta V, \quad (5.1)$$

though the provenance of this expression is not given. It is concerned mainly with terms controlling the integrated intensity of a diffraction spot and contains little which materially affects the shape. The Lorentz factor cannot in any case be used without careful consideration when  $\theta$  is very small, but values of  $\theta$  small enough to cause problems are of little interest in conventional area diffractometry. The entire content of the expression above is ignored in the equations developed below, which are concerned only with the shapes of the spots.

A tiny crystallite or mosaic block can be described as containing points within the range of (direct-space) positions denoted by the volume element  $d^3b$  at  $b$ . It is also helpful to specify mosaic misorientations lying within a restricted volume element in small-angle vector space written as, say,  $d^3\mu$  at  $\mu$ . Though the notation implies already that the volume elements are infinitesimal, strictly, each direct-space volume element is actually held to be sufficiently large that it is meaningful to use a kinematic description of its X-ray-optical properties, whilst nonetheless also being sufficiently small that no effects of internal curvature are important, either in the crystal or in the X-ray wavefront.

Whilst the sensitive surface of an area detector describes a two-dimensional space  $\mathbf{Q}^2$  in which a diffraction spot takes its shape (Thomas, 1989), a third dimension is spanned by some crystal rotation angle. This angle may be about any axis, and it is convenient to use a small-angle vector to express it as a deviation from the central diffraction position. Thus, the density of the total relative intensity of diffraction is expressed relative to a volume element  $d^2\vartheta\} d\phi$ . For gas-chamber detectors which are not always represented adequately by an equivalent (thin) assumed plane of detection, there is no objection against using  $d^3\vartheta\}$  instead of  $d^2\vartheta\}$ , though the extra complications of having to deal with an attenuating beam are not dealt with here.

The small contribution to the total scattering from this elementary volume attributable to a Bragg peak with reciprocal-lattice vector  $\mathbf{X}$  when the crystal is oriented a small angle  $\phi$  about an arbitrary axis  $\vec{\Phi}$  away from its central diffraction angle,  $\psi$ , about  $\vec{\Psi}$ , and landing a small distance,  $\vartheta\}$ , away from the central position,  $\Theta\}$ , on the detector faceplate must be describable (on an assumption of ideal imperfection so that intensities integrate linearly) by

$$\begin{aligned}
 d^{(2+1+3+3)}I &= \Sigma \begin{pmatrix} \mathbf{S} \\ \mathbf{p} \end{pmatrix} \Xi \begin{pmatrix} \mu \\ \mathbf{b} \end{pmatrix} d^2\vartheta\} d\phi\} d^3\mathbf{b}\} d^3\mu \\
 \text{tied to laboratory frame} &\longrightarrow = \Sigma \begin{pmatrix} \mathbf{R} \\ \mathbf{p} \end{pmatrix} - \frac{|\Theta+\vartheta-\mathbf{p}\rangle\langle\mathbf{R}\mathbf{R}\rangle}{2\langle\mathbf{R}\|\Theta+\vartheta-\mathbf{p}\rangle} \begin{pmatrix} \mu \\ \mathbf{b} \end{pmatrix} d^2\vartheta\} d\phi \\
 \text{tied to crystal frame} &\longrightarrow \times \Xi \begin{pmatrix} \mu \\ \mathbf{b} \end{pmatrix} d^3\mathbf{b}\} d^3\mu \\
 &= \Sigma \begin{pmatrix} \Phi\vec{\Psi}\mathbf{M}\mathbf{X} \\ \Phi\vec{\Psi}\mathbf{b} \end{pmatrix} - \frac{|\Theta+\vartheta-\Phi\vec{\Phi}\mathbf{b}\rangle\langle\mathbf{X}\mathbf{X}\rangle}{2\langle\mathbf{X}\mathbf{M}\Phi\vec{\Phi}\|\Theta+\vartheta-\Phi\vec{\Phi}\mathbf{b}\rangle} \\
 &\times \Xi \begin{pmatrix} \mu \\ \mathbf{b} \end{pmatrix} d^2\vartheta\} d\phi\} d^3\mathbf{b}\} d^3\mu, \tag{5.2}
 \end{aligned}$$

in which (3.4) has been used to refer the terms to be integrated to the crystal frame. The notation for the differential,  $d^{(2+1+3+3)}I$ , is entirely equivalent to the more usual  $d^9I$ , but makes clearer on the left-hand side the separately integrable parts on the right. The reason that integration over nine variables suffices when both  $\Sigma$  and  $\Xi$  have six arguments is that they share three because of the tight coupling between  $\mathbf{p}\}$  and  $\mathbf{b}\}$ .

The distribution function  $\Sigma$  describes completely generally the beam wave-vector distribution at all positions in direct space. In principle, it must be defined everywhere, or certainly everywhere inside the limits of integration, though it will clearly be zero well outside the main beam. It should satisfy

$$\iiint d^3\mathbf{S}\} \iiint d^3\mathbf{p}\} \Sigma \begin{pmatrix} \mathbf{S} \\ \mathbf{p} \end{pmatrix} = 1, \text{ else total beam intensity.} \tag{5.3}$$

Integrating over  $\mathbf{b}\}$  rather than over  $\mathbf{p}\}$  causes no direct

perturbation in this result since the determinant of the Jacobian relating them [a pure rotation through  $\vec{\Psi}$ , see (7.11)] is unity. The determinants of the Jacobians relating  $\mathbf{S}\}$  to  $\mu\}$  and  $\mathbf{b}\}$  are not so simple, however [cf. (7.8) and (7.12)], but, given that the entire discussion here is rather cavalier about absolute scaling, it will suffice merely to state that formally these determinants might otherwise have to be taken into account. The other distribution function,  $\Xi$ , describes the relative scattering power of each part of the crystal at each possible mosaic orientation, also in a completely general way. As for  $\Sigma$ ,  $\Xi$  should be zero when  $\mathbf{b}\}$  describes a point outside the crystal, which means that  $\Xi$  actually has to include the description of the crystal shape, and can even have this term as a separable factor if the crystal is uniform enough. It should also be the case that  $\Xi$  is vanishingly small in regions of rotational space in which a small-angle vector ceases to be an adequate representation. This is not limiting in practice. To preserve absolute scaling, it would normally be assumed that

$$\iiint d^3\mu\} \iiint d^3\mathbf{b}\} \Xi \begin{pmatrix} \mu \\ \mathbf{b} \end{pmatrix} = 1. \tag{5.4}$$

Both  $\Sigma$  and  $\Xi$  must be nowhere negative. The arrangement of the arguments of  $\Sigma$  and  $\Xi$  one above the other has no significance and is chosen only to facilitate the printing of the equations within the narrow columns of the journal. It does, however, fortuitously match the arrangement of vector terms in § 8.

## 6. The total diffraction integral

Integration of (5.2) over all positions  $\mathbf{b}\}$  and mosaic rotations  $\mu\}$  gives the total diffraction integral, which is the exact description of spot profile generation on the phonon-free kinematic model in the absence of absorption:

$$\begin{aligned}
 d^{(2+1)}I &= \iiint d^3\mathbf{b}\} \iiint d^3\mu\} d^2\vartheta\} d\phi\} \Xi \begin{pmatrix} \mu \\ \mathbf{b} \end{pmatrix} \\
 &\times \Sigma \begin{pmatrix} \Phi\vec{\Psi}\mathbf{M}\mathbf{X} \\ \Phi\vec{\Psi}\mathbf{b} \end{pmatrix} - \frac{|\Theta+\vartheta-\Phi\vec{\Phi}\mathbf{b}\rangle\langle\mathbf{X}\mathbf{X}\rangle}{2\langle\mathbf{X}\mathbf{M}\Phi\vec{\Phi}\|\Theta+\vartheta-\Phi\vec{\Phi}\mathbf{b}\rangle}. \tag{6.1}
 \end{aligned}$$



This integral displays no obviously pathological properties, but appears intractable unless constraints are placed on  $\Sigma$  and  $\Xi$ . By demanding that the beam be reasonably fine, the crystal not too large and the mosaic properties not unusual, it is then possible to offset the origin of the first (upper) argument to  $\Sigma$  and to linearize it. This linearization corresponds to the approximation of the diffraction tulip by its tangent plane at the centroid of the reversed incident-beam wave-vector distribution, which is just the mean value of  $S$ , say  $S_0$ , assumed in the previous papers.

The plane tangential to the tulip can be shown (see Appendix B) to be representable by the covector:

$$\langle U = \langle R + \langle RS|S, \quad (6.2)$$

which is so scaled that it satisfies  $\langle US \rangle = \langle RR \rangle$ . The geometry of (6.2) is shown vectorially in Fig. 7.

### 7. Derivatives of $S$

The derivatives of  $S$  with respect to  $\phi$ ,  $\psi$ ,  $b$  and  $\mu$  are all necessary for its linearization. All of these arguments are small by assumption, so it is not necessary to retain product terms.\* Instead, it is quite appropriate simply to specify that the derivatives are evaluated at the nominal central diffraction position, when  $\phi \rightarrow 0$ ,  $\psi \rightarrow 0$ ,  $b \rightarrow 0$  and  $\mu \rightarrow 0$ . The first of these forces  $\hat{\Phi} \rightarrow \mathbf{1}$ , which hence disappears from the equations.

\* The neglect of quadratic and higher terms here does not imply that the analysis of the diffractive properties of focused beams or curved crystals has been excluded; on the contrary, these effects are modelled by the completely general distributions  $\Sigma$  and  $\Xi$ . Experiments in which the crystal is absurdly large compared with the diffractometer are, however, excluded by this approximation, as are those in which the mosaicity exceeds all reasonable bounds (*i.e.* several degrees). Thus nothing of practical importance is lost.

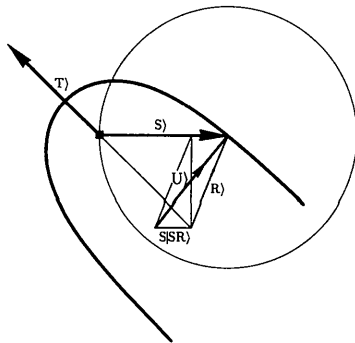


Fig. 7. The normal to the tulip. This diagram is in reciprocal space alone and uses only vector (*i.e.* no covector) constructions. It shows the normal  $U$  to the tulip at  $S$  which is just the reciprocal-lattice vector  $R$  plus its right projection onto  $S$ , given by  $S|SR$ . In order to present the normal at the point to which it applies (the centre of an Ewald sphere),  $R$  has been translated through  $-T$  from its more usual position in the diagram. The X-rays enter from the right.

A sum of two terms recurs frequently in this section and is contracted conveniently as

$$T|R = \mathbf{1} - T|R = \left[ \mathbf{1} - \frac{T\langle R \rangle}{\langle RT \rangle} \right] \quad (7.1)$$

using an asymmetric extension of the notation of the symmetry-based rotation operators (*Goniometry*). This operator has notably skew properties,  $T$  as a null right eigenvector and  $\langle R$  as a null left eigenvector:

$$T|RT = 0, \quad (7.2)$$

$$\langle RT|R = \langle 0. \quad (7.3)$$

The eigensystem of the operator is discussed in Appendix C.

The derivative of  $S$  with the simplest interpretation is that with respect to  $R$ . It is obtained directly from (3.4), but simplifies using (2.1):

$$\begin{aligned} \nabla_R S \rangle &\equiv \frac{\partial S \rangle}{\partial R \rangle} = \mathbf{1} - H|R + H|R \frac{1}{2} R|H \\ &\equiv \mathbf{1} - T|R + T|R \frac{1}{2} R|T \\ &= \mathbf{1} - T|R \frac{1}{2} R|S. \end{aligned} \quad (7.4)$$

This derivative is also notable for the skew that it induces; for example,

$$[\mathbf{1} - T|R \frac{1}{2} R|S]R = S, \quad (7.5)$$

which is not surprising since  $S$  is linearly proportional to  $R$ , whilst by symmetry

$$\langle R[\mathbf{1} - T|R \frac{1}{2} R|S] = \langle T. \quad (7.6)$$

The derivative has no effect (*i.e.* acts like the identity) on any right multiplicand (*i.e.* vector) whose inner product with  $\langle S$  vanishes and by symmetry on any left multiplicand (*i.e.* covector) whose action would annul  $T$ .

The derivative of  $R$  itself with respect to mosaic misorientations is obtained from (2.3) using techniques developed in *Goniometry*:

$$\begin{aligned} \nabla_\mu R \rangle &\equiv \frac{\partial R \rangle}{\partial \mu} = \hat{\Psi} \nabla_\mu [\hat{\mu}]X = \hat{\Psi} \nabla_\mu [X|\mu] \\ &= \hat{\Psi}[X] = \hat{\Psi}[X]\hat{\Psi}\hat{\Psi} = [R]\hat{\Psi}. \end{aligned} \quad (7.7)$$

This means that the derivative of  $S$  with respect to mosaic misorientation can now be calculated as

$$\begin{aligned} \nabla_\mu S \rangle &\equiv \frac{\partial S \rangle}{\partial \mu} = \nabla_R S \rangle \nabla_\mu R \rangle \equiv \frac{\partial S \rangle}{\partial R \rangle} \frac{\partial R \rangle}{\partial \mu} \\ &= [\mathbf{1} - T|R \frac{1}{2} R|S][R]\hat{\Psi} \\ &= [[R] + T|R[S]]\hat{\Psi} \end{aligned} \quad (7.8)$$

using the chain rule of the differential calculus and the diffraction condition (2.1) for the final reduction.

The derivative of  $S$  with respect to the detector position,  $\Theta$ , is asymmetric and dimensioned as inverse area.

It simplifies using (3.3) and (7.1):

$$\begin{aligned}\nabla_{\vartheta}\langle S\rangle &= \nabla_{\Theta}\langle S\rangle \equiv \frac{\partial S}{\partial \vartheta} = \frac{\Theta\langle RR\rangle\langle R}{\langle R\Theta\rangle 2\langle R\Theta\rangle} - \frac{\langle RR\rangle}{2\langle R\Theta\rangle}\mathbf{1} \\ &= \frac{1}{\alpha}\left[\frac{H\langle R}{\langle RH\rangle} - \mathbf{1}\right] = -\frac{T\mathbf{R}}{\alpha}.\end{aligned}\quad (7.9)$$

The derivative with respect to changes in position  $p$  within the crystal is trivially equal but opposite since  $\vartheta$  and  $p$  always appear pairwise with opposing signs:

$$\nabla_p\langle S\rangle \equiv \frac{\partial S}{\partial p} = \frac{T\mathbf{R}}{\alpha}.\quad (7.10)$$

This gives the derivative with respect to  $b$  immediately by application of

$$\nabla_b p \equiv \frac{\partial p}{\partial b} = \Psi\quad (7.11)$$

[cf. (2.8)] and the chain rule

$$\nabla_b\langle S\rangle = \nabla_p\langle S\rangle\nabla_b p = \frac{T\mathbf{R}}{\alpha}\Psi.\quad (7.12)$$

One possible route to the remaining  $\nabla_{\phi}\langle S\rangle$  would be to use  $\nabla_{\phi}p = [p]$  and  $\nabla_{\phi}R = [R]$  so that  $\nabla_{\phi}\langle S\rangle = \nabla_R\langle S\rangle\nabla_{\phi}R + \nabla_p\langle S\rangle\nabla_{\phi}p = [\mathbf{1} - T\mathbf{R}\frac{1}{2}R|S][R] + \frac{1}{\alpha}T\mathbf{R}[p] = [R] + T\mathbf{R}[S] + \frac{1}{\alpha}T\mathbf{R}[p]$ . When this derivative is calculated at the centroid of the crystal, the latter direct-space term vanishes because then  $p = 0$  by definition. The contribution from this term is, in any case, very small (of order  $\delta^2$ , say), since both  $p$  and  $\phi$  are assumed to be small (of order  $\delta$ ). A more direct route would have been to use instead the equivalence:

$$\nabla_{\phi}\mu \equiv \frac{\partial \mu}{\partial \phi} = \Psi\quad (7.13)$$

which is just the rotational operator relating the crystal and laboratory frames, so that

$$\begin{aligned}\nabla_{\phi}\langle S\rangle &= \nabla_{\mu}\langle S\rangle\nabla_{\phi}\mu = [[R] + T\mathbf{R}[S]]\Psi\Psi \\ &= [R] + T\mathbf{R}[S]\end{aligned}\quad (7.14)$$

directly from (7.8).

## 8. Examination of the total diffraction integral in Gaussian approximation

The practical evaluation of the total diffraction integral for the purpose of profile analysis is the subject of a later paper, but it is already useful to examine its behaviour under Gaussian approximation to the controlling distributions. This corresponds to the zeroth-order term in a

profile analysis using Weber-Hermite functions. Both  $\mu$  and  $b$  are naturally referred to a null vector as origin, so a Gaussian representation of the crystal in both mosaic small-angle space and in direct space is just

$$\begin{aligned}\Xi\left(\begin{matrix}\mu \\ b\end{matrix}\right) &\sim \exp\left\{-\frac{1}{2}(\mu\bar{M}\mu)\right\} \\ &\times \exp\left\{-\frac{1}{2}\{b\bar{V}b\}\right\},\end{aligned}\quad (8.1)$$

making a frequently implicit assumption that the two distributions are uncorrelated. This definition does not satisfy (5.3) and (5.4).\*

The X-ray beam can be represented in a similar way in direct space as the Gaussian:

$$\begin{aligned}\Sigma(p) &\sim \exp\left\{-\frac{1}{2}\{p\bar{P}p\}\right\} \\ &= \exp\left\{-\frac{1}{2}\{b\bar{\Psi}P\Psi b\}\right\},\end{aligned}\quad (8.2)$$

though it should be remembered that, to be a reasonable representation,  $\bar{P}$  will have an eigenvector along the beam direction with an exceedingly small eigenvalue. In principle, a rough correction for direct-beam absorption could be made by offsetting the centre about one standard deviation towards the source, but this is not done here. The overlap between the direct-space crystal and beam distributions must be narrower than either, so the two must combine to form

$$\exp\left\{-\frac{1}{2}\{b[\bar{V} + \bar{\Psi}P\Psi]b\}\right\}.\quad (8.3)$$

Again with an assumption of no correlation, the beam wave-vector distribution can be represented by

$$\Sigma(s) \sim \exp\left\{-\frac{1}{2}(s\bar{S}s)\right\},\quad (8.4)$$

where

$$\begin{aligned}s) &= \left[\frac{\partial S}{\partial \mu} \quad \frac{\partial S}{\partial b}\right] \left[\begin{matrix}\mu + \Psi\phi \\ b - \Psi\vartheta\end{matrix}\right] \\ &\equiv \delta S),\end{aligned}\quad (8.5)$$

which is referred not to the origin of wave-vector space but rather to the mean beam wave vector, say  $S_0$ . Combining these highly simplified distributions, contracted a little using matrix notation, and substituting into the total

\* It is possible to use a factor  $\pi$  rather than  $1/2$  under the exponential. This would have the desirable effect in the present context of eliminating the scaling factors of  $(2\pi)^3$  from the results, and it would also require the simpler definition of the Fourier transform lacking the factors of  $2\pi$ . There is, however, an undesirable side effect of complicating the normally factor-free equations for variance-covariance. In the full profile analysis using Weber-Hermite functions, the factor of  $\pi$  may, however, be the preferred one because of the importance of maintaining the unit normalization.

diffraction integral (6.1) gives

$$\frac{d^{(2+1)}I}{d^2\vartheta\} d\phi) \sim \iiint d^3b\} \iiint d^3\mu\} \exp\left\{-\frac{1}{2}[(\mu, \{b\} \mathcal{F} \begin{bmatrix} \mu \\ b \end{bmatrix} \right. \\ \left. - \frac{1}{2}[(\mu + \phi \dot{\Psi}, \{b - \{\vartheta \dot{\Psi}\} \mathcal{V} \begin{bmatrix} \mu + \dot{\Psi} \phi \\ b - \dot{\Psi} \vartheta \end{bmatrix} \right] \right\} \quad (8.6)$$

where

$$\mathcal{F} = \begin{bmatrix} \overline{\mathbf{M}} & \mathbf{0} \\ \mathbf{0} & \overline{\mathbf{V}} + \dot{\Psi} \overline{\mathbf{P}} \dot{\Psi} \end{bmatrix} \quad (8.7)$$

and

$$\mathcal{V} = \begin{bmatrix} \partial\langle S/\partial\mu \rangle \\ \partial\langle S/\partial\{b\} \rangle \end{bmatrix} \overline{\mathbf{S}} \begin{bmatrix} \partial S \\ \partial\mu \quad \partial\vartheta \end{bmatrix} \quad (8.8)$$

are tied to the rotating crystal. Tucking the volume element  $d^2\vartheta\} d\phi)$  under the left-hand side has no formal significance but does save space. The value of the integral is obtained by completing the squares on  $\mu)$  and on  $b)$  to get

$$\frac{d^{(2+1)}I}{d^2\vartheta\} d\phi) \sim \exp\left\{-\frac{1}{2}[(\phi \dot{\Psi}, -\{\vartheta \dot{\Psi}\} [\mathcal{V} - \overline{\mathcal{V}(\mathcal{F} + \mathcal{V})} \mathcal{V}] \begin{bmatrix} \dot{\Psi} \phi \\ -\dot{\Psi} \vartheta \end{bmatrix} \right\} \\ \times \iiint d^3b\} \iiint d^3\mu\} \exp\left\{-\frac{1}{2}[(\mu, \{b\} [\mathcal{F} + \mathcal{V}] \begin{bmatrix} \mu \\ b \end{bmatrix} \right\} \\ = \frac{(2\pi)^3}{\sqrt{|\mathcal{F} + \mathcal{V}|}} \exp\left\{-\frac{1}{2}[(\phi \dot{\Psi}, -\{\vartheta \dot{\Psi}\} [\overline{\mathcal{F} + \mathcal{V}}] \begin{bmatrix} \dot{\Psi} \phi \\ -\dot{\Psi} \vartheta \end{bmatrix} \right\}. \quad (8.9)$$

The apparently unlikely simplification of the embedded matrix,  $\mathcal{V} - \overline{\mathcal{V}(\mathcal{F} + \mathcal{V})} \mathcal{V}$ , to the intuitively expected symmetric form,  $\overline{\mathcal{F} + \mathcal{V}}$ , is explained by classical methods in Appendix A. By rearrangement of the positioning of the rotation matrices, (8.9) can be expressed more directly in terms of the detector positions  $\vartheta)$  and  $\phi)$ :

$$\frac{d^{(2+1)}I}{d^2\vartheta\} d\phi) \sim \frac{(2\pi)^3}{\sqrt{|\mathcal{F} + \mathcal{V}|}} \exp\left\{-\frac{1}{2}[(\phi, \{\vartheta\} [\overline{\mathcal{G} + \mathcal{W}}] \begin{bmatrix} \phi \\ \vartheta \end{bmatrix} \right\}, \quad (8.10)$$

where

$$\mathcal{G} = \begin{bmatrix} \dot{\Psi} \overline{\mathbf{M}} \dot{\Psi} & \mathbf{0} \\ \mathbf{0} & \dot{\Psi} \overline{\mathbf{V}} \dot{\Psi} + \overline{\mathbf{P}} \end{bmatrix}, \quad (8.11)$$

which is of full rank 6, and

$$\mathcal{W} = \begin{bmatrix} \partial\langle S/\partial\phi \rangle \\ \partial\langle S/\partial\{\vartheta\} \rangle \end{bmatrix} \overline{\mathbf{S}} \begin{bmatrix} \partial S \\ \partial\phi \quad \partial\vartheta \end{bmatrix}, \quad (8.12)$$

which, though  $6 \times 6$ , is only of rank 3.  $\mathcal{G}$  and  $\mathcal{W}$  correspond to  $\mathcal{F}$  and  $\mathcal{V}$  except in being tied to the laboratory frame. The  $6 \times 6$  matrix which forms the kernel of (8.10)

must therefore also be of full rank 6. This raises a conundrum, since the measured profiles of diffraction spots on area detectors are only three dimensional. The extra three dimensions arose because of the generality of the vectors  $\vartheta)$  and  $\phi)$ . Both are expressed quite correctly in three-dimensional spaces, though only a two-dimensional variation of the former and a one-dimensional variation of the latter will be used. This suggests that a simpler and computationally more efficient representation of (8.10) may exist. In principle, it can be created by exploiting the generalized inverses of the  $3 \times 6$  and  $6 \times 3$  Jacobians (Moore, 1920, 1935; Penrose, 1955), so that the equation assumes a form containing the required inverse of a  $3 \times 3$  matrix of full rank:

$$\begin{aligned} \overline{[\mathcal{G} + \mathcal{W}]} &= \begin{bmatrix} \partial\langle S/\partial\phi \rangle \\ \partial\langle S/\partial\{\vartheta\} \rangle \end{bmatrix} \overline{\mathbf{S} + \begin{bmatrix} \partial S \\ \partial\phi \quad \partial\vartheta \end{bmatrix}} \overline{\mathcal{G}} \begin{bmatrix} \partial\langle S/\partial\phi \rangle \\ \partial\langle S/\partial\{\vartheta\} \rangle \end{bmatrix} \\ &\times \begin{bmatrix} \partial S \\ \partial\phi \quad \partial\vartheta \end{bmatrix} \\ &= \begin{bmatrix} \partial\langle S/\partial\phi \rangle \\ \partial\langle S/\partial\{\vartheta\} \rangle \end{bmatrix} \overline{\mathbf{III}} \begin{bmatrix} \partial S \\ \partial\phi \quad \partial\vartheta \end{bmatrix}, \quad (8.13) \end{aligned}$$

though this result is secure only on the condition that  $\vartheta)$  does, indeed, span two dimensions and  $\phi)$  one. The  $3 \times 3$  matrix,  $\mathbf{III}$ , inverted at the kernel of this equation is itself just a sum of  $3 \times 3$  matrices, since  $\overline{\mathcal{G}}$ , like  $\mathcal{G}$ , is block diagonal. Expanded, it reads

$$\begin{aligned} \mathbf{III} &= \mathbf{S} + \frac{\partial S}{\partial\phi} \dot{\Psi} \overline{\mathbf{M}} \dot{\Psi} \frac{\partial S}{\partial\phi} \\ &+ \frac{\partial S}{\partial\vartheta} \dot{\Psi} \overline{\mathbf{V}} \dot{\Psi} + \overline{\mathbf{P}} \frac{\partial S}{\partial\vartheta}. \quad (8.14) \end{aligned}$$

In *Geometry*, the same symbol  $\mathbf{III}$  is used to represent the simpler quantity  $\mathbf{S} + [\mathbf{S}] \dot{\Psi} \overline{\mathbf{M}} \dot{\Psi} [\mathbf{S}]$  which is used to derive a Gaussian approximation to the angular diffraction widths of spots. The formula used the derivative  $\nabla_{\mathbf{S}} \phi = -\langle \mathbf{R}/\Upsilon$ , where  $\Upsilon$  is a signed bilinear quantity,  $\langle \mathbf{S} \Phi | \Phi \mathbf{R} \rangle$ , replacing the inverse of the conventional Lorentz factor,  $L^{-1}$ . The products of derivatives simplify considerably when back-substituted and expanded. For the angular terms [cf. (7.14)]:

$$\begin{aligned} -\Upsilon \frac{\partial\phi}{\partial\mathbf{S}} \frac{\partial\mathbf{S}}{\partial\phi} &= \langle \mathbf{R} | [\mathbf{R}] + \mathbf{T} | \mathbf{R} | [\mathbf{S}] \rangle \\ &= \langle \mathbf{R} | \mathbf{S} \rangle, \quad (8.15) \end{aligned}$$

though this result should not be interpreted as implying that  $[\mathbf{R}] + \mathbf{T} | \mathbf{R} | [\mathbf{S}]$  alone reduces to  $[\mathbf{S}]$ . The direct-space shift terms [cf. (7.9)] vanish completely:

$$-\Upsilon \frac{\partial\phi}{\partial\mathbf{S}} \frac{\partial\mathbf{S}}{\partial\vartheta} = -\langle \mathbf{R} | \frac{\mathbf{T} | \mathbf{R}}{\alpha} \rangle = \langle 0, \quad (8.16)$$

using (7.3). Thus, the old formula [*Geometry*, (11.1)] for the variance of  $\phi$  is reproduced in its original simplicity

despite the apparent complication of incorporating the effects of non-vanishing crystal and beam sizes:

$$\begin{aligned} \text{var}(\phi) \equiv \langle (\Delta\phi)^2 \rangle &= \nabla_S \phi \text{ III } \nabla_S \phi = \frac{\langle \text{RIIR} \rangle}{\Upsilon^2} \\ &= \frac{\langle \mathbf{R} \left[ \mathbf{S} + \frac{\partial \mathbf{S}}{\partial \phi} \hat{\Psi} \mathbf{M} \hat{\Psi} \frac{\partial \langle \mathbf{S} \rangle}{\partial \phi} \right. \right. \\ &\quad \left. \left. + \frac{\partial \mathbf{S}}{\partial \vartheta} \overline{\hat{\Psi} \mathbf{V} \hat{\Psi} + \mathbf{P}} \frac{\partial \langle \mathbf{S} \rangle}{\partial \vartheta} \right] \mathbf{R} \right\rangle}{\Upsilon} \\ &= \langle \mathbf{R} \frac{\mathbf{S} + [\mathbf{S}] \hat{\Psi} \mathbf{M} \hat{\Psi} [\mathbf{S}]}{\Upsilon^2} \mathbf{R} \rangle. \quad (8.17) \end{aligned}$$

This result is the physically expected one, but does depend on the assumption of lack of correlation between the various Gaussian distributions. An equivalent major simplification of the formula for the cross section of the scattered beam, in contrast, is not expected. This is because all mosaic misorientations except those whose axis is aligned along the scattering vector must stretch diffraction spots into an arc. This is borne out by the explicit equations which appear not to reduce significantly from the form created by direct substitution.

The direct-space shift equation requires a derivative of the type  $\nabla_S \vartheta$  which can be determined within an irrelevant degree of freedom by inverting the second-rank  $\nabla_S \mathbf{S}$  [(7.9)]:

$$\begin{aligned} \nabla_S \vartheta &= \left[ \nabla_S \mathbf{S} \right]^{-1} = \left[ -\frac{\overline{\mathbf{T}}\mathbf{R}}{\alpha} \right]^{-1} \\ &= -\alpha \overline{\mathbf{T}}\mathbf{R} \\ &= -\alpha \overline{\mathbf{R}}\mathbf{T}\mathbf{T}\mathbf{R}. \quad (8.18) \end{aligned}$$

Details of the inversion of  $\overline{\mathbf{T}}\mathbf{R}$  are given in Appendix C, where it is also shown that

$$\mathbf{R}\mathbf{T}\overline{\mathbf{R}}\mathbf{T} = \mathbf{T}\mathbf{T} \quad (8.19)$$

and hence by transposition

$$\overline{\mathbf{T}}\mathbf{R} \mathbf{T}\mathbf{R} = \mathbf{T}\mathbf{T}. \quad (8.20)$$

Equations (8.19) and (8.20) allow a minor simplification of the direct-space equation of scattered-beam cross section developed below. Any reduction of the contribution from mosaicity to the same equation would rely on a further reduction of the form of (7.14)  $(\nabla_S \mathbf{S}) = [\mathbf{R}] + \mathbf{T}\mathbf{R}[\mathbf{S}]$  and although there are several rearrangements, the author has not been able to find one with fewer than two components.\* Thus, the direct-space spot-shape equation in

\* The product,  $\mathbf{R}\mathbf{T} \left[ [\mathbf{R}] + \mathbf{T}\mathbf{R}[\mathbf{S}] \right] = \mathbf{R}\mathbf{T} \left[ [\mathbf{R}] + \mathbf{S}\mathbf{R}[\mathbf{S}] \right]$ , but this equation is not valid in the absence of the prefactor  $\mathbf{R}\mathbf{T}$ . Equation (8.21) does contain this prefactor within the symbol  $\overline{\mathbf{T}}\mathbf{R}$  so this rearrangement could be used, but offers little advantage.

Gaussian approximation appears to be irreducible beyond

$$\begin{aligned} \text{var}(\vartheta) &= \nabla_S \vartheta \text{ III } \nabla_S \vartheta \\ \rightarrow &= \alpha \overline{\mathbf{T}}\mathbf{R} \text{ III } \overline{\mathbf{R}}\mathbf{T}\alpha \\ &= \alpha \overline{\mathbf{T}}\mathbf{R} \left[ \mathbf{S} + \frac{\partial \mathbf{S}}{\partial \phi} \hat{\Psi} \mathbf{M} \hat{\Psi} \frac{\partial \langle \mathbf{S} \rangle}{\partial \phi} \right. \\ &\quad \left. + \frac{\partial \mathbf{S}}{\partial \vartheta} \overline{\hat{\Psi} \mathbf{V} \hat{\Psi} + \mathbf{P}} \frac{\partial \langle \mathbf{S} \rangle}{\partial \vartheta} \right] \overline{\mathbf{R}}\mathbf{T}\alpha \\ &= \alpha \overline{\mathbf{T}}\mathbf{R} \mathbf{S} \overline{\mathbf{R}}\mathbf{T}\alpha \\ &\quad + \alpha \overline{\mathbf{T}}\mathbf{R} \left[ [\mathbf{R}] + \mathbf{T}\mathbf{R}[\mathbf{S}] \right] \hat{\Psi} \mathbf{M} \hat{\Psi} \left[ [\mathbf{R}] + [\mathbf{S}]\mathbf{R}\mathbf{T} \right] \overline{\mathbf{R}}\mathbf{T}\alpha \\ &\quad + \mathbf{T}\mathbf{T} \overline{\hat{\Psi} \mathbf{V} \hat{\Psi} + \mathbf{P}} \mathbf{T}\mathbf{T}. \quad (8.21) \end{aligned}$$

The rearrangements of this equation make use of (8.18), (8.14), (7.14), (7.19), (8.19) and (8.20) in that order. The variance of  $\vartheta$  along the direction of the scattered beam,  $\mathbf{T}$ , is not defined by (8.21); it is in any case undefined to the extent of being indefinitely large. The first term of the final expression represents the divergence of the scattered beam between the crystal and the detector; the second term represents the extra smearing of spots because of mosaicity; the third term represents the beam shape just as it leaves the crystal. Although this result seems to suggest that even in Gaussian approximation the shape of the outgoing beam is far from simple, a comparison of the arrowed expression in (8.21) with (8.17) does display a possibly surprising remaining orthogonality and, indeed, an economy of representation. The angular term (8.17) is obtained by probing III with the single vector  $\mathbf{R}$  (a rank 1 probe), whereas the beam shape (8.21) is obtained by probing III with directions strictly orthogonal to  $\mathbf{R}$  (a rank 2 probe). This must actually be a forced result of using (8.13). If only the angular equation is considered, the deponent form of III ( $= \mathbf{S} + [\mathbf{S}] \hat{\Psi} \mathbf{M} \hat{\Psi} [\mathbf{S}]$ ) suffices, and not only always has the same form, but for a single position of the crystal even has the same value for all diffraction spots. This means that it used to be considered as an 'honorary' second-rank tensor, despite being an obviously contrived quantity (Thomas, 1992). A consideration of the beam shape, however, demolishes this interpretation because it does not seem to be possible to disentangle the variation of the full form of III from the reciprocal-lattice vector,  $\mathbf{R}$ ).

The equations developed above show unambiguously that the beam divergence and the mosaicity affect the shapes of diffraction spots in different ways. On an area diffractometer, the effects are distinguishable because the full three-dimensional profile is perceivable. Observation of a single spot, or even several neighbouring ones, to arbitrarily high accuracy cannot determine the controlling distributions. When, however, a major part of the entire diffraction pattern is available, it becomes feasible to determine these various contributions. This opens the possibility of a full analytically justifiable three-dimensional profile analysis for area diffractometers which will be developed in a subsequent paper.

### Concluding remarks

This is the most detailed analysis of the geometrical generation of diffraction-spot profiles yet developed for use with an area-detector diffractometer or camera, and it is hoped that it will be of value in the development of formally justifiable profile-analysis algorithms. The direct relationship between the detailed properties of the beam and of the crystal have been shown explicitly, though it has not yet been possible to explore fully the complications introduced by phonon coupling or by absorption. The present analysis should, however, provide a sufficiently good basis on which to verify some of the assumptions made by currently available profile-analysis algorithms which rely on the local similarity of the geometry.

The quartic diffraction tulip and the equivalent cam in direct space are not thought to have been reported previously.

The author is grateful to Dr P. A. Tucker and especially to Dr Robert Diamond for helpful comments on the manuscript. Much of the preliminary work leading to this paper was supported by the Medical Research Council of Great Britain as part of the development of the Enraf-Nonius FAST system, and was completed at the European Molecular Biology Laboratory supported by an EMBO long-term fellowship.

### APPENDIX A

#### The simultaneous diagonalization of two matrices

The author is indebted to Dr Richard Bryan for pointing out that the identity relation used in § 8 can be proved without using the convolution theorem by exploiting the fact that two real symmetric positive-definite matrices can be diagonalized simultaneously. This is perhaps easier to understand in geometrical terms, when such matrices are representable by ellipsoidal contours. The metric can be altered so that one ellipsoid becomes isometric, in other words circular, spherical or hyperspherical depending on the number of dimensions. The other matrix can then be represented in diagonalized form in the normal way by exploiting rotations which, because of the change of metric, do not upset the diagonalization of the first matrix. It is obviously not generally possible to achieve simultaneous diagonalization of more than two matrices.

The straightforward diagonalization of a matrix, say  $\mathbf{B}$ , can be expressed as

$$\mathbf{B} = \mathbf{S}\mathbf{N}\mathbf{S} \iff \mathbf{B}\mathbf{S} = \mathbf{S}\mathbf{N} \iff \mathbf{S}\mathbf{B}\mathbf{S} = \mathbf{N} \quad (A1)$$

where  $\mathbf{S}$  and its inverse  $\mathbf{S}$  are rotation matrices, so that

$$\mathbf{S}\mathbf{S} = \mathbf{1} = \mathbf{S}\mathbf{S} \quad (A2)$$

and  $\mathbf{N}$  is the diagonal matrix of eigenvalues  $\nu$  written in quite sufficient detail as  $\mathbf{N} = \text{diag}(\nu)$ . Using  $\mathbf{M}$  to control

the metric, it must be possible to write

$$\mathbf{M}^T\mathbf{A}\mathbf{M} = \mathbf{M}^T\mathbf{B}\mathbf{M} \text{diag}(\lambda) = \mathbf{M}^T\mathbf{B}\mathbf{M}\mathbf{A} \quad (A3)$$

where  $\lambda$  are the eigenvalues of the diagonal  $\mathbf{A}$ . To achieve simultaneous diagonalization of  $\mathbf{A}$  and  $\mathbf{B}$ , this equation is forced to look the same as (A1) by setting  $\mathbf{M}^T\mathbf{B}\mathbf{M} = \mathbf{1}$ , which implies directly that

$$\mathbf{B} = \overline{\mathbf{M}}^T\overline{\mathbf{M}}, \quad (A4)$$

constraining  $\mathbf{M}$  within an arbitrary unitary factor. This is the first result necessary to prove the initial assertion about simultaneous diagonalization.  $\mathbf{M}$  is not singular, so the  $\mathbf{M}^T$  in (A3) can be removed by premultiplying with  $\overline{\mathbf{M}}^T$ . Then  $\mathbf{B}$  can be substituted from (A1), giving

$$\mathbf{A}\mathbf{M} = \mathbf{S}\mathbf{N}\mathbf{S}\mathbf{M}\mathbf{A} \quad (A5)$$

and hence  $\mathbf{S}\mathbf{A}\mathbf{S}\mathbf{S}\mathbf{M} = \mathbf{N}\mathbf{S}\mathbf{M}\mathbf{A}$  using (A2). This can be rephrased in a way that generates the unknown unitary factor:

$$\overline{\mathbf{N}}^{\frac{1}{2}}\mathbf{S}\mathbf{A}\mathbf{S}\overline{\mathbf{N}}^{\frac{1}{2}} \underbrace{\mathbf{N}^{\frac{1}{2}}\mathbf{S}\mathbf{M}}_{\mathbf{Y}} = \underbrace{\mathbf{N}^{\frac{1}{2}}\mathbf{S}\mathbf{M}}_{\mathbf{Y}} \mathbf{A}, \quad (A6)$$

which is of the same form as (A1) provided that  $\mathbf{Y}\mathbf{Y} = \mathbf{1} = \mathbf{Y}\mathbf{Y}$  (in other words, that  $\mathbf{Y}$  is indeed unitary) and  $\mathbf{A} = \text{diag}(\lambda)$ , which has been specified already in (A3).  $\mathbf{N}^{\frac{1}{2}}$  is never unique, but this is of no importance since any correct form is equally valid. Rearranging the (repeated) braced term in (A6) gives the expression for  $\mathbf{M}$ :

$$\mathbf{M} = \mathbf{S}\overline{\mathbf{N}}^{\frac{1}{2}}\mathbf{Y}, \quad (A7)$$

which, being substituted into  $\mathbf{A} = \mathbf{S}\mathbf{N}\mathbf{S}\mathbf{M}\mathbf{A}\overline{\mathbf{M}}$  from (A5), by expansion and cancellation reduces to

$$\mathbf{A} = \overline{\mathbf{M}}^T\mathbf{A}\overline{\mathbf{M}}, \quad (A8)$$

which is the second result necessary to prove the assertion about simultaneous diagonalization.

The identity sought can now be proved by substituting the values for  $\mathbf{A}$ ,  $\mathbf{B}$ , and exploiting the diagonalization to rearrange to a symmetric form:

$$\begin{aligned} \mathbf{B} - \mathbf{B}(\mathbf{A} + \mathbf{B})\mathbf{B} &= \overline{\mathbf{M}}^T\overline{\mathbf{M}} - \overline{\mathbf{M}}^T\overline{\mathbf{M}} \left[ \overline{\mathbf{M}}^T\mathbf{A}\overline{\mathbf{M}} + \overline{\mathbf{M}}^T\overline{\mathbf{M}} \right]^{-1} \overline{\mathbf{M}}^T\overline{\mathbf{M}} \\ &= \overline{\mathbf{M}}^T\overline{\mathbf{M}} - \overline{\mathbf{M}}^T [\mathbf{A} + \mathbf{1}]^{-1} \overline{\mathbf{M}} \\ &= \overline{\mathbf{M}}^T [\mathbf{1} - \text{diag}(1/[1 + \lambda])] \overline{\mathbf{M}} \\ &= \overline{\mathbf{M}} [\mathbf{1} - \text{diag}(1/[1 + \lambda])]^{-1} \overline{\mathbf{M}}^T \\ &= \overline{\mathbf{M}} [\text{diag}(\lambda/[1 + \lambda])]^{-1} \overline{\mathbf{M}}^T \\ &= \overline{\mathbf{M}} [\text{diag}([1 + \lambda]/\lambda)] \overline{\mathbf{M}}^T \\ &= \overline{\mathbf{M}} [\text{diag}(1/\lambda) + \mathbf{1}] \overline{\mathbf{M}}^T \\ &= \overline{\mathbf{M}}\overline{\mathbf{A}}\overline{\mathbf{M}}^T + \overline{\mathbf{M}}\overline{\mathbf{M}}^T \\ &= \overline{\mathbf{A}} + \overline{\mathbf{B}}. \end{aligned} \quad (A9)$$

### APPENDIX B

#### The normal to the surface of the tulip

The Jacobian of  $\langle S \rangle$  with respect to  $\langle R \rangle$  will generate only vectors within the tangent plane of the tulip at  $\langle S \rangle$  if the changes in  $\langle R \rangle$  are perpendicular to  $\langle R \rangle$  itself. This is easily arranged by introducing any non-zero power of  $|\langle R \rangle|$  or of  $\langle R \rangle$ ;  $\langle R \rangle$  is used here:

$$\begin{aligned} \nabla_{\langle R \rangle} \langle S \rangle \langle R \rangle &= [\mathbf{1} - \langle T \rangle \langle R \rangle \frac{1}{2} \langle S \rangle] \langle R \rangle \\ &= \langle R \rangle - \langle T \rangle \langle R \rangle \frac{1}{2} [\langle R \rangle - \langle R \rangle \langle T \rangle] \\ &= \langle R \rangle - \langle T \rangle \langle R \rangle \frac{1}{2} \langle T \rangle. \end{aligned} \quad (B1)$$

This latter operator must have the normal to the surface of the tulip as a left null eigenvector. Because of the cylindrical symmetry of the tulip, this covector must be expressible as a linear combination of two of  $\langle R \rangle$ ,  $\langle S \rangle$  or  $\langle T \rangle$ , no vector out of their plane being required. Setting the covector to be

$$\langle U \rangle = \alpha \langle S \rangle + \beta \langle R \rangle \quad (B2)$$

gives

$$[\alpha \langle S \rangle + \beta \langle R \rangle] [\langle R \rangle - \langle T \rangle \langle R \rangle \frac{1}{2} \langle T \rangle] = \langle 0 \rangle \quad (B3)$$

as the eigenequation required. Expanding this and gathering terms in  $\langle S \rangle$  and in  $\langle R \rangle$ , which must null separately, shows that

$$\alpha = \frac{\langle RS \rangle}{\langle SS \rangle} \beta. \quad (B4)$$

Setting  $\beta \leftarrow 1$  and hence  $\alpha \leftarrow \langle RS \rangle / \langle SS \rangle$  gives (6.2) directly.

### APPENDIX C

#### The inversion of $\langle T \rangle \langle R \rangle$

Equation (7.9) contains the matrix operator  $\langle T \rangle \langle R \rangle$  whose inverse is required in (8.21). The classical inverse does not exist, but the generalized inverse (Moore, 1920, 1935; Penrose, 1955) can be formed as

$$\overline{\langle T \rangle \langle R \rangle} = \overline{\langle R \rangle \langle T \rangle \langle R \rangle} \langle R \rangle \langle T \rangle \quad (C1)$$

or, equally, as

$$\overline{\langle T \rangle \langle R \rangle} = \langle R \rangle \langle T \rangle \overline{\langle R \rangle \langle R \rangle \langle T \rangle} \quad (C2)$$

(cf. Appendix B in *Geometry*). The forms  $\langle R \rangle \langle T \rangle \langle R \rangle$  and  $\langle T \rangle \langle R \rangle \langle R \rangle \langle T \rangle$  are real symmetric positive matrices. Only one, say  $\langle R \rangle \langle T \rangle \langle R \rangle$ , need be considered in detail because the results for the other can be found simply by swapping  $\langle R \rangle$  and  $\langle T \rangle$ . It is clear from (7.2) that  $\langle T \rangle$  is a null eigenvector of  $\langle R \rangle \langle T \rangle \langle R \rangle$ :

$$\langle R \rangle \langle T \rangle \langle R \rangle \langle T \rangle = \langle 0 \rangle, \quad (C3)$$

whilst from (7.1) any vector perpendicular both to  $\langle R \rangle$  and

to  $\langle T \rangle$ , say  $\langle T \rangle \langle T \rangle \langle R \rangle$ , is a unit eigenvector:

$$\langle R \rangle \langle T \rangle \langle R \rangle \langle T \rangle \langle T \rangle \langle R \rangle = \langle T \rangle \langle T \rangle \langle R \rangle. \quad (C4)$$

The third eigenvector must be perpendicular to the first two and can be chosen consistently as  $\langle T \rangle \langle T \rangle \langle R \rangle$ . The form  $\langle R \rangle \langle T \rangle \langle R \rangle \langle T \rangle \langle T \rangle \langle R \rangle$  does not reduce by an obvious route to the required form  $\langle T \rangle \langle T \rangle \langle R \rangle \lambda$ , where  $\lambda$  is the eigenvalue. The eigenvalue can, however, be found because if  $\mathbf{M} \mathbf{v} = \mathbf{v} \lambda$ , where  $\mathbf{M}$  is a matrix and  $\mathbf{v}$  an eigenvector, then  $\lambda = \mathbf{v}^T \mathbf{M} \mathbf{v} / \mathbf{v}^T \mathbf{v}$ . Using this rule and reducing the formula by direct substitution and expansion gives

$$\begin{aligned} \lambda &= \frac{\langle \langle R \rangle \langle T \rangle \langle R \rangle \langle T \rangle \langle T \rangle \langle R \rangle \rangle}{\langle \langle R \rangle \langle T \rangle \langle T \rangle \langle T \rangle \langle R \rangle \rangle} \\ &= \frac{\langle \langle RR \rangle \rangle \langle \langle TT \rangle \rangle}{\langle \langle RT \rangle \rangle \langle \langle TR \rangle \rangle}. \end{aligned} \quad (C5)$$

The inverse of  $\langle R \rangle \langle T \rangle \langle R \rangle$  can now be created explicitly as a sum of rank 1 matrices with inverted eigenvalues. For a generalized inverse, a null eigenvalue does not invert divergently but remains null. Thus, the inverse is a sum of only two terms picking out the subspace normal to the null eigenvector  $\langle T \rangle$ :

$$\begin{aligned} \overline{\langle R \rangle \langle T \rangle \langle R \rangle} &= \frac{\langle T \rangle \langle TR \rangle \langle RT \rangle \langle T \rangle}{\langle \langle RT \rangle \langle T \rangle \langle T \rangle \langle TR \rangle \rangle} + \frac{\langle T \rangle \langle TR \rangle \bar{\lambda} \langle RT \rangle \langle T \rangle}{\langle \langle RT \rangle \langle T \rangle \langle T \rangle \langle TR \rangle \rangle} \\ &= \frac{\langle T \rangle \langle TR \rangle \langle RT \rangle \langle T \rangle}{\langle \langle RT \rangle \langle TR \rangle \rangle} + \frac{\langle T \rangle \langle TR \rangle \bar{\lambda} \langle RT \rangle \langle T \rangle}{\langle \langle RT \rangle \langle TR \rangle \rangle}, \end{aligned} \quad (C6)$$

where

$$\bar{\lambda} = \frac{\langle \langle RT \rangle \rangle \langle \langle TR \rangle \rangle}{\langle \langle RR \rangle \rangle \langle \langle TT \rangle \rangle}. \quad (C7)$$

The product of the original matrix  $\langle R \rangle \langle T \rangle \langle R \rangle$  with its inverse is

$$\langle R \rangle \langle T \rangle \langle R \rangle \overline{\langle R \rangle \langle T \rangle \langle R \rangle} = \langle T \rangle \langle T \rangle, \quad (C8)$$

which differs from the identity,  $\mathbf{1}$ , by having  $\langle T \rangle$  as a null eigenvector. Simply regrouping the factors in (C8) gives

$$\langle R \rangle \langle T \rangle \overline{\langle R \rangle \langle T \rangle} = \langle T \rangle \langle T \rangle, \quad (C9)$$

which is used in the direct-space part of (8.21).

#### References

- ARNDT, U. W. & PHILLIPS, D. C. (1961). The linear diffractometer. *Acta Cryst.* **14**, 807–818.
- ARNDT, U. W. & WONACOTT, A. J. (1977). *The Rotation Method in Crystallography*, edited by U. W. ARNDT & A. J. WONACOTT. Amsterdam: North-Holland.
- BRAGG, W. L. (1913). The diffraction of short electro-magnetic waves by a crystal. *Proc. Cambridge Philos. Soc.* **17**, 43–57.
- BURKE, W. L. (1985). *Applied Differential Geometry*. Cambridge Univ. Press.

- BUSING, W. R. & LEVY, H. A. (1967). Angle calculations for 3- and 4-circle X-ray and neutron diffractometers. *Acta Cryst.* **22**, 457-464.
- DIAMOND, R. (1969). Profile analysis in single crystal diffractometry. *Acta Cryst.* **25**, 43-55.
- DIRAC, P. A. M. (1958). *The Principles of Quantum Mechanics*, 4th ed., §§ 5-6, pp. 14-22 (bra-ket notation) and § 15, pp. 58-61 (delta function). Oxford Univ. Press.
- EWALD, P. P. (1913). Zur Theorie der Interferenzen der Röntgenstrahlen in Kristallen. *Phys. Z.* **14**, 465-472.
- KABSCH, W. (1988). Evaluation of single-crystal X-ray diffraction data from a position-sensitive detector. *J. Appl. Cryst.* **21**, 916-924.
- LIPSON, H. (1972). *International Tables for X-ray Crystallography*, Vol. II, p. 265, equations (11). Birmingham: Kynoch Press. (Present distributor Kluwer Academic Publishers, Dordrecht.)
- MOORE, E. H. (1920). On the reciprocal of the general algebraic matrix [abstract]. *Bull. Am. Math. Soc.* **26**, 394-395.
- MOORE, E. H. (1935). *General Analysis*. Philadelphia: American Philosophical Society.
- PENROSE, R. (1955). A generalized inverse for matrices. *Proc. Cambridge Philos. Soc.* **51**, 406-413.
- RICHMOND, T. J., FINCH, J. T., RUSHTON, B., RHODES, D. & KLUG, A. (1984). Structure of the nucleosome core particle at 7 Å resolution. *Nature (London)*, **311**, 532-537.
- THOMAS, D. J. (1982). Fast diffractometry. PhD thesis, Cambridge Univ., England.
- THOMAS, D. J. (1989). Calibrating an area-detector diffractometer: imaging geometry. *Proc. R. Soc. London Ser. A*, **425**, 129-167.
- THOMAS, D. J. (1990a). Calibrating an area-detector diffractometer: integral response. *Proc. R. Soc. London Ser. A*, **428**, 181-214.
- THOMAS, D. J. (1990b). Modern equations of diffractometry. Goniometry. *Acta Cryst.* **A46**, 321-343.
- THOMAS, D. J. (1992). Modern equations of diffractometry. Diffraction geometry. *Acta Cryst.* **A48**, 134-158.
- WONACOTT, A. J. (1977). Geometry of the rotation method. *The Rotation Method in Crystallography*, edited by U. W. ARNDT & A. J. WONACOTT, ch. 7, pp. 75-103. Amsterdam: North-Holland.

*Acta Cryst.* (1993). **A49**, 460-467

## Simulation of X-ray Topographs: a New Method to Calculate the Diffracted Field

BY C. A. M. CARVALHO AND Y. EPELBOIN

Laboratoire de Minéralogie-Cristallographie, Universités P. M. Curie et Paris VII, UA 009,  
CNRS, Case 115, 75252 Paris CEDEX 05, France

(Received 21 July 1992; accepted 8 October 1992)

### Abstract

The precision of the numerical algorithms used to integrate the Takagi-Taupin equations has been in the past a severe limitation for the simulation of accurate topographs. The intensity, especially in the direct image of the defect, is underestimated. This has forbidden the use of the reciprocity theorem for the simulation of traverse and white-beam synchrotron topographs. A new algorithm is described, based on two different methods of expressing the partial-derivative equations, which permits a faster and more accurate calculation.

### I. Introduction

X-ray topography is a widespread method for single-crystal characterization. Computer simulation of topographs is useful for image interpretation because it allows quantitative analysis of the perfection of crystals. The comparison between the computed and the experimental images makes it possible to test the validity of a deformation model for the defects seen in the image and to determine quantitatively parameters that are not accessible through the experiment such as the sign and magnitude of the Burgers vector of a dislocation or the nature of a stacking fault. Simulation of section topographs is now well established (Epelboin, 1985). As for traverse topographs,

Petrashen, Chukovskii & Shulpina (1980) have attempted to calculate the intensity along a line of the image and Epelboin & Soyer (1985) have simulated whole images. The latter have shown that the precision of the algorithms was not sufficient for the reciprocity theorem of optics to be used as suggested by Petrashen (1976).

Three aspects must be considered when computing X-ray topographs:

- (i) the kind of wave incident on the surface of the crystal;
- (ii) the numerical method to solve the propagation equations inside the crystal;
- (iii) the network of integration used to integrate these equations.

Let us briefly review each of them. X-ray topography may be classified into two groups: plane-wave and spherical-wave topography. Laboratory and synchrotron-radiation sources produce spherical waves (Aristov, Kohn, Polovinkina & Snigirev, 1982; Carvalho & Epelboin, 1990), so that to obtain a plane wave it is necessary to put a specially designed monochromator in front of the specimen. Petrashen *et al.* (1980) explained why the most efficient method to simulate plane-wave topographs is the Tournarie method (Authier, Malgrange & Tournarie, 1968). Thus, in this paper we will study only the case of the spherical wave, *i.e.* section and traverse topographs.